Meas. Sci. Technol. **23** (2012) 015101 (11pp) doi:10.1088/0957-0233/23/1/015101

Piezoelectric, solar and thermal energy harvesting for hybrid low-power generator systems with thin-film batteries

P Gambier[1], S R Anton[2], N Kong[3], A Erturk[4,6] and D J Inman[5]

[1] Institut Supérieur de l'Aéronautique et de l'Espace, Toulouse, CEDEX 31055, France
[2] The Engineering Institute, Los Alamos National Laboratory, Los Alamos, NM 87545, USA
[3] Texas Instruments Inc., Manchester, NH 03101, USA
[4] G W Woodruff School of Mechanical Engineering, Georgia Institute of Technology, Atlanta, GA 30332, USA
[5] Department of Aerospace Engineering, University of Michigan, Ann Arbor, MI 48109, USA

E-mail: alper.erturk@me.gatech.edu

Received 11 July 2011, in final form 5 October 2011
Published 25 November 2011
Online at stacks.iop.org/MST/23/015101

Abstract
The harvesting of ambient energy to power small electronic components has received tremendous attention over the last decade. The research goal in this field is to enable self-powered electronic components for use particularly in wireless sensing and measurement applications. Thermal energy due to temperature gradients, solar energy and ambient vibrations constitute some of the major sources of energy that can be harvested. Researchers have presented several papers focusing on each of these topics separately. This paper aims to develop a hybrid power generator and storage system using these three sources of energy in order to improve both structural multifunctionality and system-level robustness in energy harvesting. A multilayer structure with flexible solar, piezoceramic, thin-film battery and metallic substructure layers is developed (with the overhang dimensions of 93 mm × 25 mm × 1.5 mm in cantilevered configuration). Thermal energy is also used for charging the thin-film battery layers using a 30.5 mm × 33 mm × 4.1 mm generator. Performance results are presented for charging and discharging of the thin-film battery layers using each one of the harvesting methods. It is shown based on the extrapolation of a set of measurements that 1 mA h of a thin-film battery can be charged in 20 min using solar energy (for a solar irradiance level of 223 W m^{-2}), in 40 min using thermal energy (for a temperature difference of 31 °C) and in 8 h using vibrational energy (for a harmonic base acceleration input of 0.5g at 56.4 Hz).

Keywords: energy harvesting, power scavenging, vibrational energy, thermal energy, solar energy, power conditioning, hybrid systems, multimodal systems, multifunctional structures

(Some figures in this article are in colour only in the electronic version)

1. Introduction

Harvesting of waste energy for powering small electronic components (such as wireless sensor networks used in monitoring applications) has received significant attention in recent years. The eventual goal in this research field is to enable self-powered electronic components so that the maintenance costs and the chemical waste resulting from the use and replacement of conventional batteries can be minimized. Thermal, solar, wind and vibrational energy can be converted to usable electrical energy for powering such remote electronic devices autonomously [1]. Solar panels are used for converting incident light (usually sunlight) into electricity through the photovoltaic effect [2] whereas thermoelectric generators (TEGs) are employed for

[6] Author to whom any correspondence should be addressed.

transforming thermal gradients into electricity through the Seebeck effect [3]. Wind energy can be converted into low-power electricity using small-scale windmills [4] or aeroelastic flutter [5]. Piezoelectric, electromagnetic, electrostatic and magnetostrictive transduction mechanisms can be employed for converting vibrations into electricity [6–10]. However, due to their large power density, ease of application and relative ease of fabrication at micro-scale, piezoelectric materials have been most heavily researched for vibration-to-electricity conversion [1, 11, 12]. This paper focuses on combined solar, thermoelectric and piezoelectric energy harvesting through the multifunctional self-charging structure concept in order to develop hybrid low-power generator systems with thin-film batteries.

The concept of multifunctionality in material systems aims to combine several essential functions into a single material or component to improve the overall performance of a system. Through the combination of multiple functionalities in a single material, redundant materials can be eliminated from a system, resulting in improvements to the weight and volume of the structure. Some of the earlier efforts in multifunctional material systems are reviewed in the literature [13] with details on the development of structural power material systems, autonomous sensing and actuating material systems, electromagnetic multifunctional material systems and survivable, damage-tolerant material systems. Of these four classes of multifunctional material systems, structural power systems, which integrate structural function with energy storage ability, are of most interest for energy harvesting applications. Some of the original work on structural power systems involves the creation of lightweight structural materials for use in spacecraft applications with embedded batteries for energy storage [14]. Researchers have more recently investigated the integration of lithium polymer batteries into structural composite materials to create structural batteries for use in unmanned vehicle applications [15].

Hybrid (or multimodal) energy harvesting, in which energy is captured from several ambient sources, is another concept that can be applied to improve upon conventional energy harvesting designs. The ability to harvest from several sources of ambient energy provides robustness against varying environmental conditions, effectively allowing the system to remain online in the case where ambient energy is no longer available from one or more of the sources. Previous research has investigated simultaneous harvesting of vibration energy using the direct piezoelectric effect and harvesting of magnetic energy (alternating magnetic fields) using magnetostrictive materials bonded to piezoelectric layers, effectively creating magnetoelectric composites [16]. Simultaneous harvesting of vibration energy using electromagnetic transduction and thermal energy using TEGs has also been reported in the literature [17].

The recently introduced concept of self-charging structures [18] combines flexible piezoceramic, thin-film battery and metallic layers to develop multifunctional structures that can sustain dynamic loads, generate electricity (as a result of structural excitation under dynamic loading) and store the electricity in itself for use in low-power applications. The self-charging structure concept is aimed to improve the existing concept of multifunctionality [13–15] by combining both the generator and the storage capabilities within the load-bearing structure. Anton *et al* [18] fabricated prototypes of these self-charging structures, showed the feasibility of charging the battery layers using the piezoelectric output under dynamic base excitation (in a cantilevered configuration) and tested the strength of the assembly as well as its individual layers through three-point bending tests.

This paper aims to extend the self-charging structure concept to include solar and thermal energy harvesting as well so that the concepts of multifunctionality and hybrid energy harvesting are combined. In addition to the flexible piezoceramic, thin-film battery and metallic layers, flexible solar layers are used to fabricate a multifunctional composite structure with symmetric layers. Kapton layers are used for electrical isolation while high-shear strength epoxy layers are used in a vacuum bonding process during fabrication. The resulting assembly is tested under base excitation for piezoelectric energy harvesting and is also exposed to simulated sunlight for solar energy harvesting. The electrical outputs are regulated in nonlinear power conditioning circuits and used for charging the thin-film battery layers. As another component of the setup, thermal energy is also used for charging the thin-film battery layers. A conventional TEG is used in this study with the eventual goal of incorporating novel flexible TEGs directly into the self-charging structure assembly. Charge and discharge time histories are given for the independently conducted energy harvesting tests using these three energy harvesting techniques and the results are discussed.

2. An overview of the configuration and fabrication of the assembly

2.1. Experimental setup

The experimental setup used in this work is shown in figure 1. The cantilevered assembly with flexible aluminum, piezoceramic, thin-film battery and solar layers is clamped onto the armature of an electromagnetic shaker. The acceleration at the base of the cantilever (i.e. on the armature of the shaker) is measured using a small accelerometer for the vibration-based energy harvesting experiments. The outermost layers of the cantilevered assembly are the solar layers. Sunlight is simulated using a solar spectrum metal halide light and the irradiance level is measured using an irradiance sensor near the upper surface of the cantilever. A heat source and a heat sink are attached onto the hot side and the cold side of the TEG, respectively, and two thermocouples are used for recording the temperature values on both faces of the generator. For charging a thin-film battery layer, the electrical outputs of the thermoelectric, solar and piezoelectric generators are connected independently to their power conditioning circuits under certain temperature difference, solar irradiance and vibration levels. The regulated circuit outputs are connected directly to the thin-film batteries in consecutive experiments.

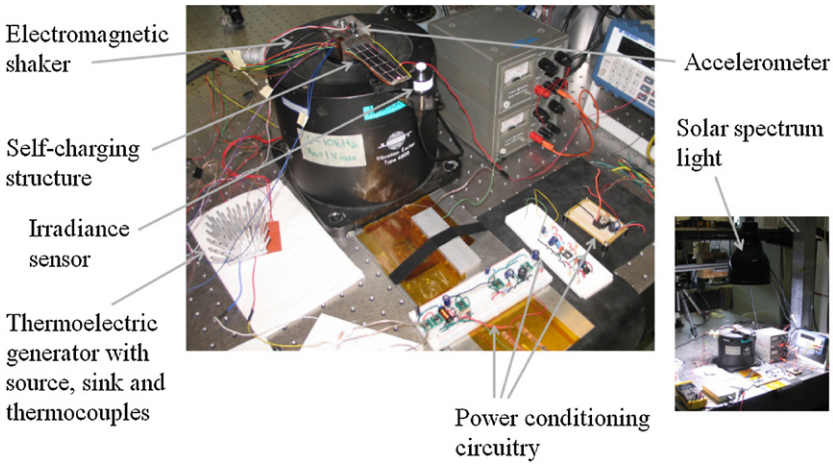

Figure 1. Experimental setup used for piezoelectric, solar and thermal energy harvesting.

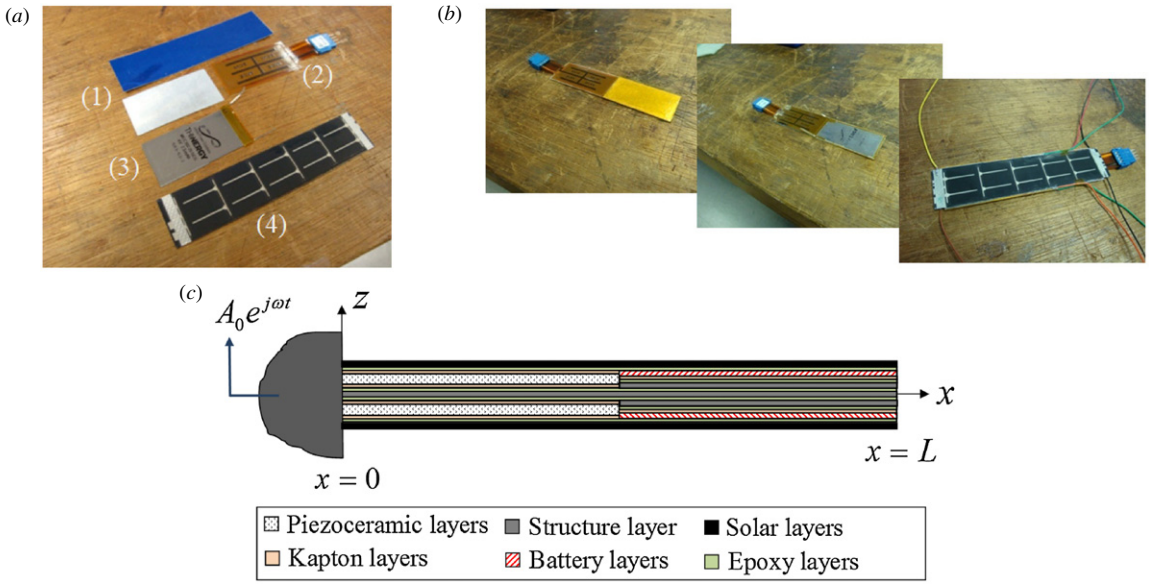

Figure 2. (*a*) Components of the flexible self-charging assembly: (1) aluminum substructure, (2) piezoceramic layer in Kapton material, (3) flexible battery layer, (4) flexible solar layer; (*b*) fabrication stages of the assembly (the assembly is symmetric with respect to the central aluminum layer); (*c*) a schematic of the assembly under harmonic base excitation.

2.2. Components and fabrication of the flexible self-charging structure

The main components of the self-charging structure are the flexible aluminum, piezoceramic, battery and solar layers as shown in figure 2(*a*) and the major fabrication stages of one side of the symmetric assembly are displayed in figure 2(*b*). The piezoelectric devices used in this study are QuickPack QP10n piezoceramics manufactured by Midé Technology Corporation, which include a central PZT-5A layer bracketed in Kapton with embedded flexible copper electrodes. Flexible thin-film battery layers (MEC102) from Infinite Power Solutions, Inc., are used for energy storage and are composed of a metal foil substrate (which acts as the electrode surface) with active layers including lithium-metal anodes, lithium cobalt dioxide ($LiCoO_2$) cathodes and lithium phosphorus oxynitride (LiPON) electrolyte layers. The solar panels used in this work are flexible panels manufactured by PowerFilm, Inc., which contain amorphous silicon printed on a polymer substrate in a roll-to-roll manufacturing process. An idealized schematic of the assembly is depicted in figure 2(*c*), where the piezoceramic layers are located at the clamped side while the battery layers are at the free end of the cantilever. Flexible thin-film batteries and solar panels offer a significant advantage over their conventional counterparts (supercapacitors/lithium polymer batteries and polycrystalline solar panels, respectively) in the fact that they are extremely thin and flexible devices, allowing them to be directly integrated into self-charging structures. Moreover, thin-film batteries offer high cycle life and low leakage. Additional Kapton layers (not shown in figure 2(*a*)) are used in the assembly to avoid shorting of the battery layers to the substrate. High-shear strength epoxy (3M-DP460) is used in the vacuum bonding process (which is described elsewhere [18] in detail). The main aluminum (Al 1100) substrate is 0.127 mm thick and its length and width under

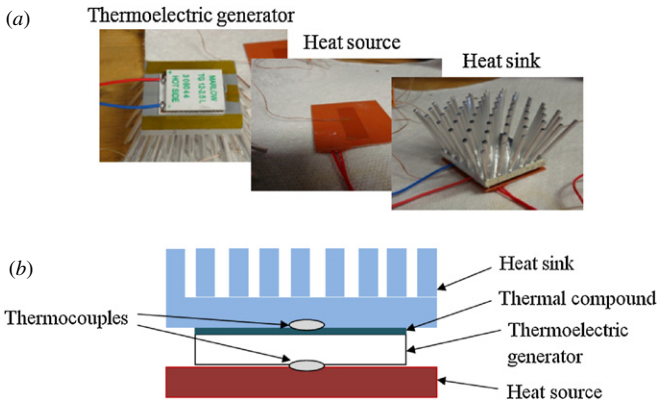

Figure 3. (*a*) Thermoelectric power generator with its heat source, heat sink and thermocouples and (*b*) a schematic representation.

unclamped condition are 101.6 by 25.4 mm, respectively. Each piezoceramic with its Kapton layers is 0.381 mm thick, 50.8 mm long and 25.4 mm wide while the thickness of each battery layer is 0.178 mm with the same length-to-width ratio. An additional 0.203 mm aluminum layer is therefore used for increasing the thickness of the battery region. The solar layers are 0.178 mm thick, 114.3 mm long (with 99 mm solar cell length) and 25.4 mm wide. Including the epoxy and the Kapton layers, the overall dimensions of the composite assembly under clamped condition are approximately 93 mm × 25 mm × 1.5 mm (while the region with the battery layers has slightly different thickness as compared to that with the piezo layers due to the additional Kapton films included to avoid shorting of the battery layers). Note that the TEG (with its heater and cooler) is not directly a part of the flexible self-charging assembly.

3. Basic characterization of the system components

3.1. Thermoelectric power output

The components of the thermal energy harvesting setup are shown in figure 3(*a*). The TEG used in the experiments is a 30.5 mm × 33.0 mm × 4.1 mm Bi_2Te_3 TEG module (TG 12-2.5-01 L—Marlow Industries, Inc.). The module can convert waste heat into DC power for temperatures less than 200 °C with maximum reliability according to the manufacturer. The hot side of the TEG is located on a flexible heating pad and a heat sink (cooler) is attached to the cold side by means of a thermal compound. The thermal compound (RCX-TC060—Rosewill, Inc.) used for attaching the heat sink to the TEG is chosen among the alternatives to maximize the thermoelectric power output for the same heater input. As depicted in figure 3(*b*), two thermocouples are used to record the temperature values on the hot and cold sides of the TEG.

Several heat sinks are compared to maximize the thermoelectric power output for the same levels of power input to the heater (figure 4(*a*)). The same type of thermal compound (RCX-TC060—Rosewill, Inc.) is used in the comparisons. Two of the five heat sinks investigated here (3-202014G and 3-202016G (both nickel plated aluminum)—Cool Innovations) use natural convection cooling while the other three (4-1818042 (copper), 3-1818042, 3-181802 (both nickel plated aluminum)—Cool Innovations) use fans in addition to fins. In the comparison process, the voltage input to the heater is gradually increased (which alters the temperature difference across the generator) and the power output of the TEG is recorded for a 10 Ω resistive load (which is approximately the matched electrical resistance of the TEG). Figure 4(*b*) shows the variation of the thermoelectric power output for different levels of temperature difference. It turns out from this graph that the heat sink 3-202016G (that employs natural convection cooling) results in the largest power output among the heat sinks tested for this particular setup. Note that no specific forced air convection is applied to the heat sinks in the experiments. The manufacturer's reported thermal resistance for the chosen heat sink (3.22 °C W^{-1}) is also found to match the thermal resistance of the TEG well (which is in the range 3.33–3.58 °C W^{-1} for various values of temperature difference in the manufacturer's data sheet). This is in agreement with the discussion given by Mayer and Ram [19] to optimize the thermoelectric power output (through equating the temperature difference between the heat source and the sink and the temperature difference between the sink and the ambient for the maximum power transfer).

Having chosen the heat sink, resistor sweep measurements are carried out for different voltage levels of the heater plate (yielding different heat flux levels) as shown in figure 5. The resulting average temperature difference (ΔT) values

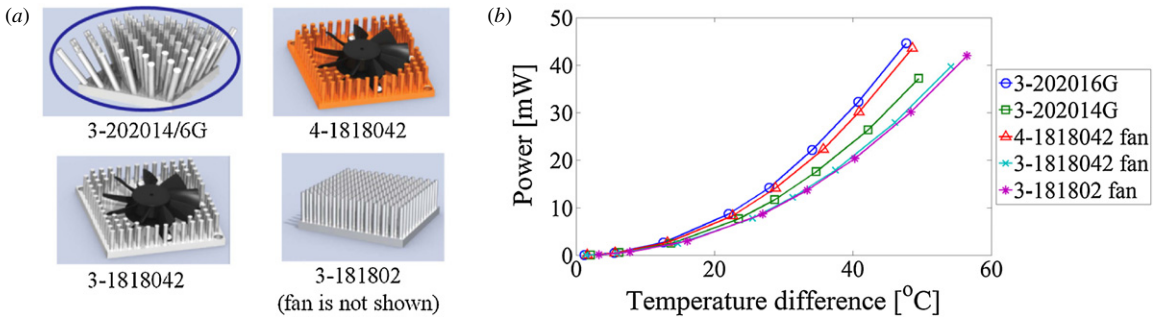

Figure 4. (*a*) Various types of heat sinks using natural convection and fans compared in this study (the selected heat sink is encircled) and (*b*) their comparison in terms of the maximum thermoelectric power output for different levels of power input to the same heater (yielding different temperature difference levels) using the same TEG and thermal compound.

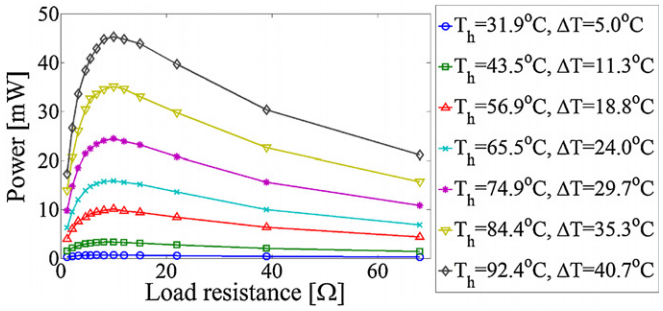

Figure 5. Power output versus load resistance diagrams of the TEG for different values of the average hot side temperature and the resulting average temperature difference (legends show the average values for the set of resistors in each curve).

range from 5.0 to 40.7 °C. The term *average* is used for the ΔT values because the temperature difference across the generator (particularly the hot side temperature, T_h) changes with changing load resistance for a fixed heater input (i.e. heat flux). For instance, for the lowest heat flux case, the temperature difference for an electrical load close to short-circuit conditions (1.2 Ω) is 4.5 °C whereas the open-circuit temperature difference is 5.5 °C. It is also observed from figure 5 that the matched resistance (approximately 10 Ω) does not change significantly with changing temperature difference across the TEG. Using the TEG shown in figure 3(*a*), a raw DC power output of 45 mW can be extracted for a temperature difference of about 41 °C. The open-circuit voltage output of the TEG strongly depends on the temperature difference. For the range of temperature differences covered here, it is observed that the open-circuit voltage output changes from 0.15 V (for the lowest temperature difference) to 1.4 V (for the highest temperature difference). As expected [20], the electrical load of the maximum power output shown in figure 5 is very close to the electrical resistance of the TEG reported by the manufacturer (in the range of 9–11 Ω for different values of the temperature difference).

3.2. Solar power output

The flexible self-charging cantilever described in section 2.2 is located under a solar spectrum light (6500 K—Hamilton Technology) while an irradiance sensor (SRS-100—Pace Scientific, Inc.) records the level of irradiance near the cantilever (located on the shaker) as shown in figure 6(*a*). The focus is placed on the outermost solar layer on the upper surface as it is directly exposed to the incident light. The irradiance reading depends on the proximity of the solar layer from the solar spectrum light. This distance is altered to achieve three levels of irradiance (124, 311 and 437 W m^{-2}) in order to determine the electrical output over a range of solar input conditions, and resistor sweep tests are run to obtain the maximum electrical power output of a single layer. Figure 6(*b*) shows that the matched resistance of the solar layer depends dramatically on the irradiance level. An irradiance level of 437 W m^{-2} results in a raw DC power output of 30 mW from the top solar panel of the self-charging structure. The open-circuit voltage output of the solar layer changes from 3.8 to 4 V as the irradiance level changes from 124 to 437 W m^{-2}.

3.3. Piezoelectric power output

The crucial information for the vibration-based energy harvesting experiments is the fundamental resonance frequency of the cantilevered self-charging assembly in order to generate the maximum piezoelectric power output under resonance excitation. Using the electromagnetic shaker, the small accelerometer and the data acquisition system shown in figure 7(*a*), the voltage output-to-base acceleration frequency response functions [12, 21, 22] of the cantilevered self-charging structure are obtained for a set of resistive loads ranging from the short-circuit to the open-circuit conditions (figure 7(*b*)). The electrodes of the piezoceramic layers are combined in parallel for improved current output. The frequency range of 0–500 Hz covers the first two bending modes [12] of the cantilever as shown in figure 7(*b*) (where the base acceleration is normalized with respect to the gravitational acceleration, $g = 9.81$ m s^{-2}). For every excitation frequency, the voltage across the load increases monotonically with increasing load resistance. Expectedly, the electrical output that can be extracted from the fundamental vibration mode is much larger than that of the second vibration mode; hence the focus is placed on the first bending mode of the cantilever.

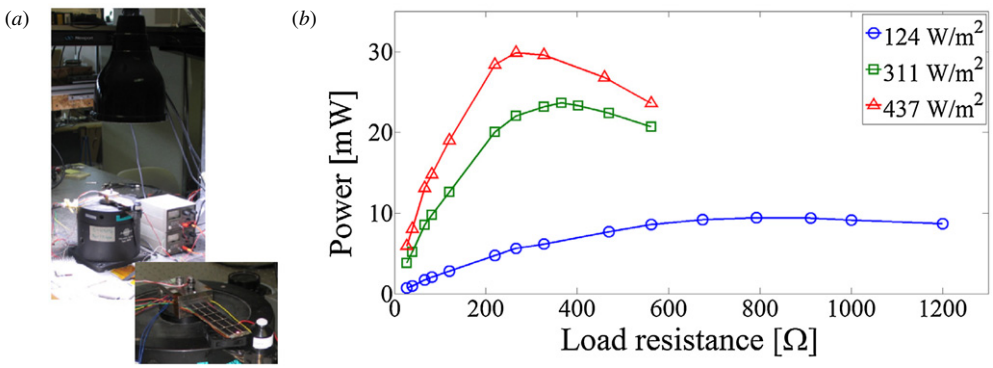

Figure 6. (*a*) Close-up view of the experimental setup showing the solar spectrum light at the top and the irradiance sensor near the cantilever; (*b*) power output versus load resistance of a single solar layer (the top layer) for different irradiance levels.

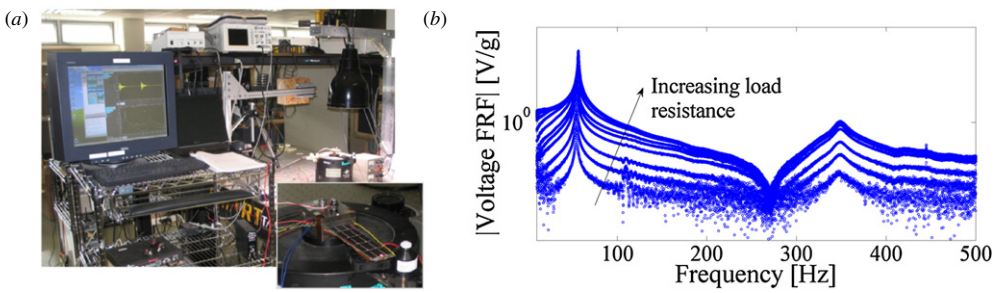

Figure 7. (*a*) Experimental setup used for electromechanical modal analysis for piezoelectric energy harvesting and (*b*) the voltage output-to-base acceleration frequency response functions for a set of resistive loads ranging from the short-circuit to open-circuit conditions.

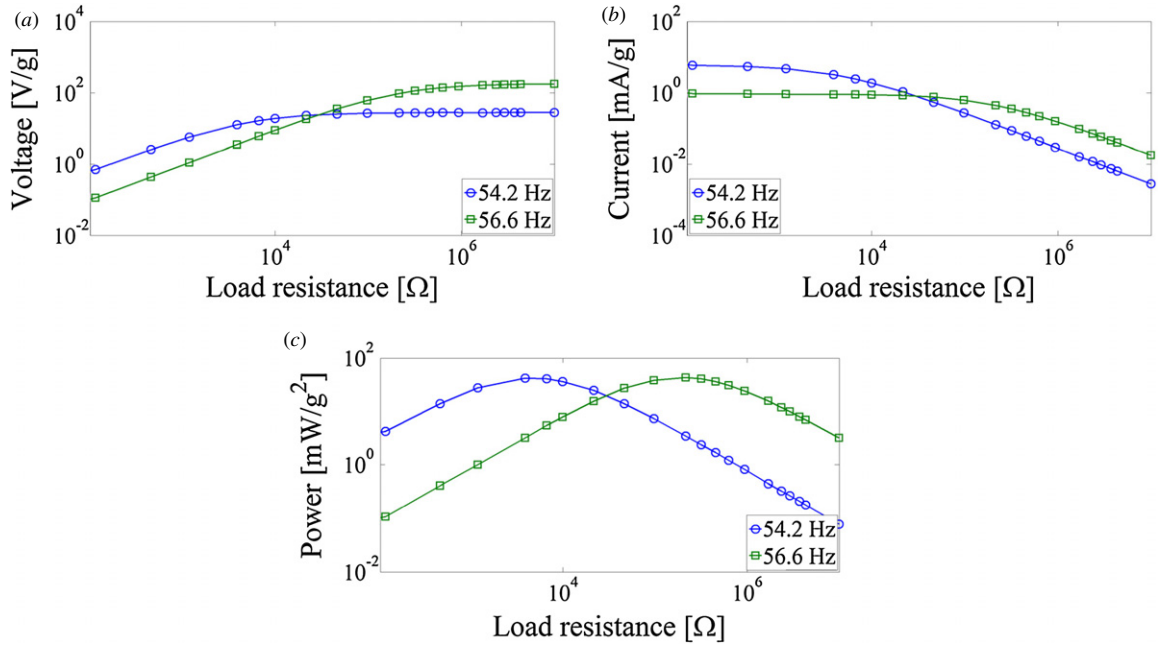

Figure 8. Performance diagrams for piezoelectric energy harvesting: (*a*) voltage amplitude versus load resistance, (*b*) current amplitude versus load resistance, (*c*) power amplitude versus load resistance (per base acceleration) for excitation at the fundamental short-circuit (circles) and open-circuit (squares) resonance frequencies.

As the external load is increased from the short-circuit to the open-circuit conditions, the resonance frequency of the fundamental vibration mode moves from approximately 54.2 to 56.6 Hz, which are the fundamental short-circuit and open-circuit resonance frequencies, respectively [12, 21, 22]. For harmonic excitations at these two frequencies, the variations of the AC electrical outputs (per base acceleration in g) are plotted against the load resistance in figure 8. Figures 8(*a*) and (*b*), respectively, display the AC voltage and current amplitudes while figure 8(*c*) shows the AC power amplitude. The linear peak power estimate is approximately 40 mW g^{-2} (which is a linear approximation valid for relatively low base acceleration levels and it may overestimate the power output significantly for high base acceleration inputs due to material and dissipative nonlinearities [23, 24]). This approximation means 0.4 mW AC power amplitude (non-rectified and unregulated) for 0.1g base acceleration amplitude at the fundamental short-circuit or the open-circuit resonance frequencies. Note that the optimum resistive load of the maximum power output strongly depends on the excitation frequency (figure 8(*c*)).

4. Power conditioning circuits and charging of the battery layers

4.1. Two-stage circuits for thermal and solar energy harvesting

In most energy harvesting applications, the amount of scavenged energy is too low to directly power a load; hence an intermediate storage stage is required. This typically does not present a problem when powering wireless sensor nodes as they usually operate on a low duty cycle, perhaps only needing to operate a few times each month. In order to convert the raw power output of the energy harvesting sources to a stable DC power to be stored in the thin-film battery, an efficient power conditioning circuit is indispensible for energy harvesting. In this paper, a two-stage power conditioning circuit is implemented for both the TEG and the solar layer(s). The schematic of this two-stage circuit is shown in figure 9. The first stage of the circuit is a buck-boost converter to provide an interface with matched impedance for the maximum power extraction. The second stage of the circuit is a linear regulator

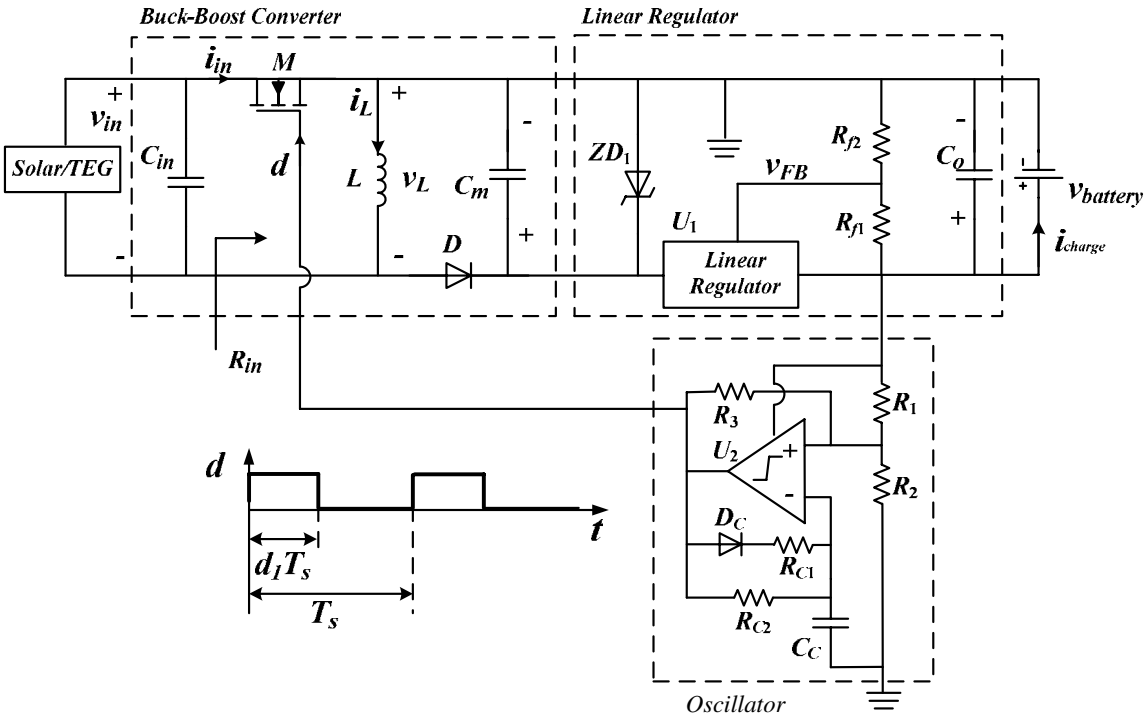

Figure 9. Power conditioning circuit for thermal and solar energy harvesting.

to control the output voltage at the appropriate level suggested for charging the thin-film battery. The Thinergy MEC102 batteries used in this work have a rated voltage of 4.0 V, a capacity of 2.5 mA h and the manufacturer recommends charging the batteries with a potential of 4.1 V.

The buck-boost converter running in discontinuous conduction mode is inherently a natural lossless resistor. The equivalent input impedance of the buck-boost converter shown in figure 9 is a function of the inductance value L, the switching frequency T_S and the duty cycle d_1. These parameters can be adjusted to match the source impedance for the maximum output power extraction. In this circuit, a low-power comparator (U_2) with an RC network is used to generate the gate signal to drive the power MOSFET M. Details of the oscillator circuit can be found in Kong *et al* [25].

4.2. Single-stage circuit with a rectifier for piezoelectric energy harvesting

For typical base acceleration inputs, the electrical power generated from the vibrations of the piezoceramic layers is much less than the power outputs of thermoelectric and solar generators (for the temperature difference and solar irradiance levels considered here). As a result, power dissipation in the relatively complex switching-mode converter [25, 26] may overwhelm the power gain of the impedance matching interface. Therefore, the power conditioning circuit for piezoelectric energy harvesting implemented here includes the minimum necessary circuitry: a rectifier and a linear voltage regulator. The circuit schematic used for piezoelectric energy harvesting is shown in figure 10.

Table 1. Circuit parameters for thermal, solar and piezoelectric energy harvesting.

Thermal		Solar		Piezoelectric	
d_1	0.42	d_1	0.17	–	–
D	PMEG2005	D	1N8517	–	–
L	RFB1010-101 L	L	RFB1010-221 L	–	–
M	RTQ020N03	M	RTQ020N03	–	–
T_S	112 μs	T_S	40 μs	–	–
U_1	TPS71501	U_1	TPS71501	U_1	TPS71501
U_2	TLV3491	U_2	TLV3491	U_3	MB1 S

4.3. Circuit parameters

Following the preliminary analysis of the raw electrical outputs given in section 3, the optimum resistive load that maximizes the average DC power output is first identified by tuning the load resistor manually for the three different energy harvesting sources. Then the circuit components and parameters are chosen for impedance matching and voltage regulation. The key circuit parameters are listed in table 1.

5. Charge–discharge experiments and discussion of the results

5.1. Charge and discharge experiments

Three different energy harvesting sources are consecutively connected to a single battery layer through the aforementioned power conditioning circuits for an independent set of charge–discharge experiments. Each test is performed for an arbitrary amount of time and the tests are not intended to fully charge the battery (if fully charged, the battery

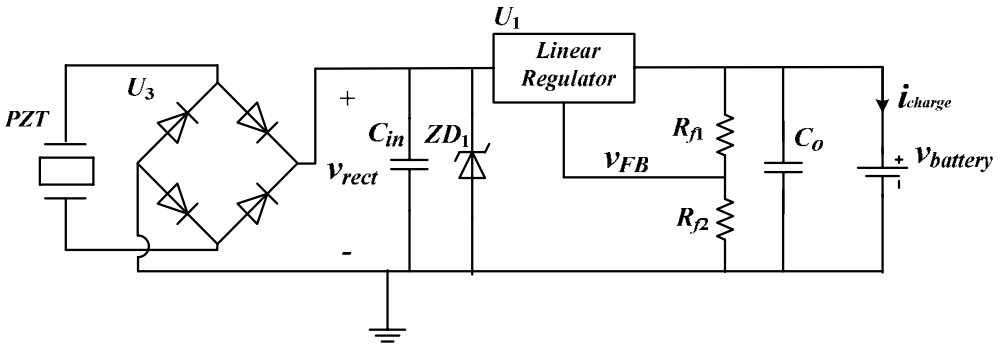

Figure 10. Power conditioning circuit for piezoelectric energy harvesting.

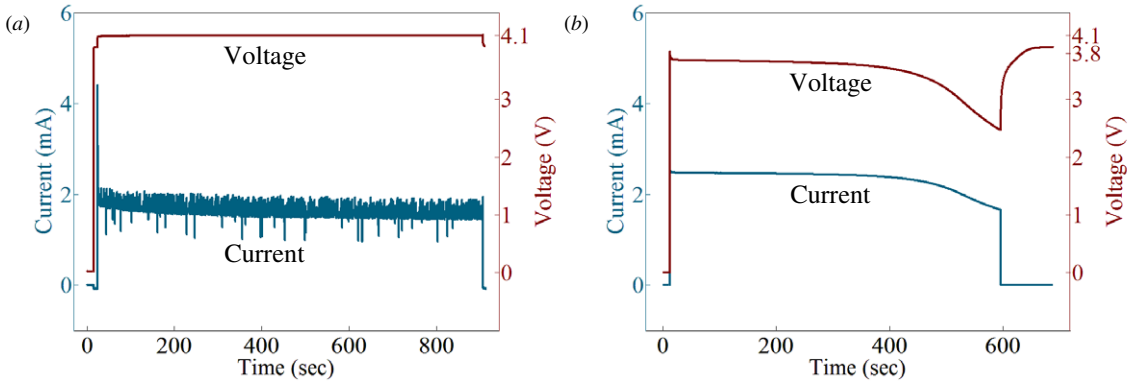

Figure 11. (*a*) Current and voltage histories for charging 0.40 mA h of a single battery in 15 min using the thermoelectric power output due to 31 °C temperature difference and (*b*) the discharge histories.

could enter a trickle charge state, thus distorting the output power calculations). The ambient energy levels used in the testing (e.g. temperature differential, solar irradiance, vibration amplitude and frequency) are selected in order to simulate realistic ambient conditions for each mode of harvesting. In the thermal and solar energy harvesting experiments, discharging is performed by applying a resistive load of 1.5 kΩ across the battery in order to draw roughly 2.5 mA of current (corresponding to a 1 C discharge rate) until a voltage level of 2.5 V is reached. In the piezoelectric energy harvesting experiment, a smaller 0.7 mA h capacity thin-film battery external to the self-charging structure is used (MEC-101—Infinite Power Solutions, Inc.) to better match the low-power output of the harvester such that a fair percentage of the battery can be charged in a reasonable amount of time. A Keithley 2611A SourceMeter is used to sink a constant 1.4 mA of current (corresponding to 2 C) from the battery during discharging until a voltage level of 3 V is reached. All discharge tests are performed with the harvester disconnected from the circuit in order to assess the amount of energy stored in the harvesting tests. Both the voltage and current are recorded for the thermal and solar energy harvesting tests using a National Instruments Corporation CompactDAQ data acquisition system with an NI 9215 analog voltage input card with 16-bit precision. Current measurements are made using a transimpedance amplifier to convert current into a measurable voltage. For the piezoelectric energy harvesting test, the voltage and current are measured directly with the Keithley SourceMeter.

For the thermal energy harvesting experiments, the temperature difference between the hot and the cold sides is set equal to 31 °C. The thin-film battery receives an average DC power of 6.6 mW for this temperature difference. The voltage and current histories for 15 min of charging time are shown in figure 11(*a*). The charge capacity of the battery is estimated as 0.40 mA h by integrating the current measurement over time. The voltage and current histories associated with discharging are shown in figure 11(*b*). The discharge capacity is obtained from the area under the current curve shown in figure 11(*b*) as 0.37 mA h. The small difference between the calculated charge and discharge capacity levels is attributed to possible current leakage associated with charging.

For an irradiance level of 223 W m^{-2}, close to the average irradiance level found on the Earth's surface in the United States [27], the battery receives 12.5 mW average DC power from the power conditioning circuit of the solar panel. Figure 12(*a*) shows the voltage and current histories for charging a thin-film battery layer with this power input for 26 min, yielding a charge capacity of 1.3 mA h. The discharge time histories are given in figure 12(*b*), where the discharge capacity is 1.2 mA h.

In the presence of the nonlinear piezoelectric energy harvesting circuit (figure 10), the resonance frequency of the cantilevered self-charging structure is measured as 56.4 Hz. For harmonic base excitation with an acceleration amplitude of 0.5*g* at 56.4 Hz, the battery receives an average DC power of 0.49 mW. Figure 13(*a*) shows the voltage and current histories

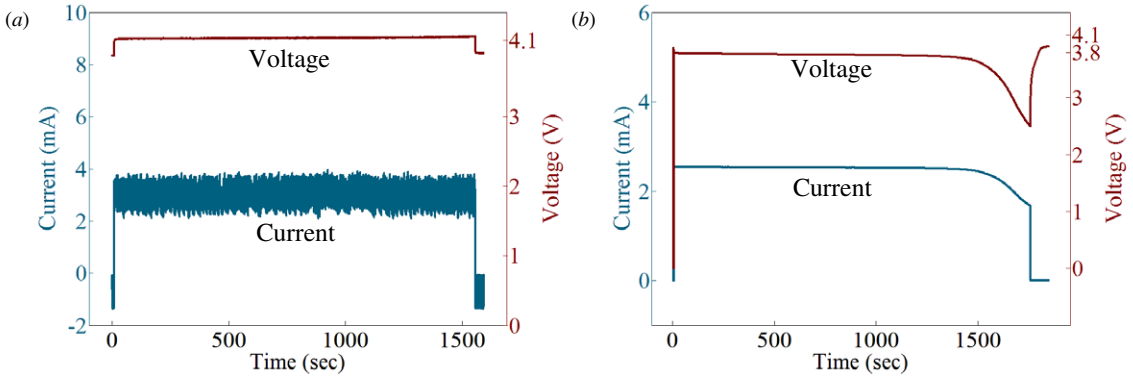

Figure 12. (*a*) Current and voltage histories for charging 1.3 mA h of a single battery in 26 min using the solar power output due to the 223 W m^{-2} irradiance level and (*b*) the discharge histories.

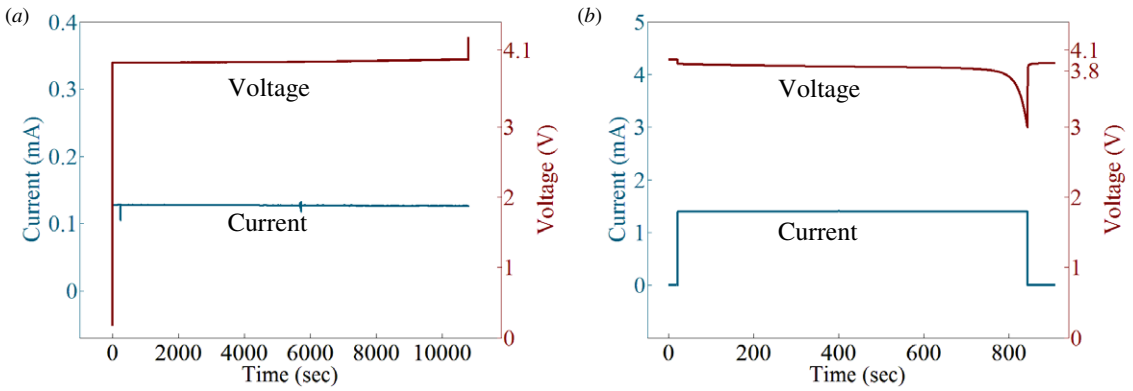

Figure 13. (*a*) Current and voltage histories for charging 0.38 mA h of a single battery in 3 h using the piezoelectric power output with 0.5*g* base acceleration at 56 Hz and (*b*) the discharge histories.

for charging 0.38 mA h of capacity for a single battery layer in 3 h. It can be observed from the figure that for a reasonable input vibration level, the piezoelectric current output is more than an order of magnitude less compared to the current produced in the thermal and solar experiments, thus reducing the average DC power received by the battery drastically. A drawback of piezoelectric harvesting is its inherently low-power output for typical ambient conditions when compared to solar and thermal harvesting. The discharge voltage and current time histories are shown in figure 13(*b*), yielding the discharge capacity of 0.32 mA h.

5.2. Extrapolation and discussion of the results

Table 2 shows a summary of the battery charging experiments with an extrapolation to estimate the duration of charging 1 mA h of a thin-film battery for the configurations considered in this section. The charge durations given in figures 11(*a*), 12(*a*) and 13(*a*) are taken as the basis in this extrapolation. For instance, since 0.40 mA h of a single thin-film battery is charged in 15 min in the thermal energy harvesting case, the linear extrapolation yields 40 min for charging 1 mA h with the same input (i.e. temperature difference). Similar extrapolations listed in table 2 exhibit that solar energy harvesting requires the least amount of time as well as the least volume. A single flexible solar layer can charge 1 mA h of the battery in only 20 min. Expectedly, vibration-based energy harvesting requires the longest duration for charging the same capacity level under resonant excitation (8 h for 1 mA h capacity). Considering the volumetric effect (i.e. charge capacity divided by volume and charge duration), it is obvious that solar energy is substantially superior. Thermoelectric component appears to be close to the solar component in terms of the charge duration when the size effect is ignored. However, it is important to note that the effectiveness of thermal energy harvesting strongly depends on the temperature difference (figure 5) and the value of 31 °C is chosen arbitrarily here. Recall that the advantage of the hybrid concept discussed herein is the robustness against varying environmental conditions so that the energy harvesting system remains online in case ambient energy is not available from one or more of the sources. For instance, although the 8 h required for charging the same capacity with vibrational energy might seem substantially longer than the solar case, this situation can have practical value if these hours correspond to the absence of sunlight during the day.

6. Conclusions

A multifunctional hybrid energy harvesting system is investigated experimentally. In addition to flexible thin-film battery and piezoceramic layers, flexible solar layers

Table 2. Extrapolated data for estimating the full charging duration of 1 mA h using thermal, solar and vibrational energy.

	Thermal	Solar	Vibrational
Input	Temperature difference: 31 °C	Irradiance: 223 W m^{-2}	Base acceleration: 0.5*g* at 56.4 Hz
Dimensions	30.5 mm × 33 mm × 4.1 mm (excluding the sink)	93 mm × 25 mm× 0.178 mm (single layer)	93 mm × 25 mm × 1.5 mm (cantilevered volume)
Volume	4.13 cm^3	0.414 cm^3	3.49 cm^3
Duration of charging 1 mA h	40 min	20 min	8 h

are combined with an aluminum substructure to construct a multilayer self-charging structural configuration that can generate electricity from dynamic loads and sunlight, and store the electrical energy in its flexible thin-film battery layers. Thermoelectric power output is also used for charging the thin-film battery layers using a conventional TEG, with the eventual goal of incorporating novel thin-film flexible thermoelectric devices directly into the self-charging structure assembly. Nonlinear energy harvesting circuits are used for converting the raw DC outputs in thermal and solar energy harvesting and the raw AC output in piezoelectric energy harvesting to the stable DC output required for charging the thin-film battery layers. The goals of the hybrid energy harvesting concept that employs a composite structure with thin-film storage components are to improve robustness in energy harvesting through the ability of harvesting multiple energy sources and multifunctionality through the load bearing capability of the flexible structure.

The flexible composite cantilever used for solar and piezoelectric energy harvesting with its battery layers has the approximate dimensions of 93 mm × 25 mm × 1.5 mm under clamped conditions while the TEG has the dimensions of 30.5 mm × 33 mm × 4.1 mm. For a temperature difference of 31 °C between the hot and the cold sides of the TEG, the thin-film battery receives a regulated DC power of 6.6 mW, charging 0.40 mA h of capacity in 15 min. An irradiance level of 223 W m^{-2} results in 12.5 mW regulated DC power flowing into the thin-film battery from one flexible solar panel, charging 1.3 mA h of capacity in 26 min. For a base acceleration input of 0.5*g* at 56.4 Hz, the thin-film battery layer receives 0.49 mW regulated DC power from the piezoceramic layers, charging 0.38 mA h of capacity in 3 h. Expectedly, the current output of piezoelectric layers is much lower than those of the thermoelectric and solar generators. Therefore the regulated DC power output in piezoelectric energy harvesting is more than an order of magnitude lower as compared to those of the other two energy harvesting techniques. The extrapolated results based on these measurements imply that 1 mA h of a thin-film battery can be charged in 20 min using solar energy (for a solar irradiance level of 223 W m^{-2}), in 40 min using thermal energy (for a temperature difference of 31 °C) and in 8 h using vibrational energy (for a base acceleration input of 0.5*g* at 56.4 Hz).

Although the battery charging experiments are conducted independently for the three energy harvesting techniques discussed in this paper, it is required to combine the circuitry for simultaneous harvesting of the thermal, solar and piezoelectric energy. One practical difficulty in implementing these techniques simultaneously is the amount of wiring. Using printed circuits to minimize wiring can be considered as a future research topic. Moreover, flexible electronics can be combined with the flexible self-charging structure. Recently developed fiber-based flexible TEGs can also be combined with the flexible self-charging structure depending on the application (i.e. if the hot and cold domains allow and if the other layers are not negatively affected by the temperature levels).

Acknowledgments

The experiments were conducted in the Center for Intelligent Material Systems and Structures at Virginia Tech. The authors gratefully acknowledge the support from the US Air Force Office of Scientific Research under the grant F9550-06-1-0326 'Energy Harvesting and Storage Systems for Future Air Force Vehicles' monitored by Dr B L Lee.

References

[1] Cook-Chennault K A, Thambi N and Sastry A M 2008 Powering MEMS portable devices—a review of non-regenerative and regenerative power supply systems with emphasis on piezoelectric energy harvesting systems *Smart Mater. Struct.* **17** 043001

[2] Miles R W, Hynes K M and Forbes I 2005 Photovoltaic solar cells: an overview of state-of-the-art cell development and environmental issues *Prog. Cryst. Growth Charact. Mater.* **51** 1–42

[3] Chen M, Lu S S and Liao B 2005 On the figure of merit of thermoelectric generators *ASME J. Energy Resour. Technol.* **127** 37–41

[4] Priya S, Chen C T, Fye D and Zahnd J 2005 Piezoelectric windmill: a novel solution to remote sensing *Japan. J. Appl. Phys.* **44** L104–7

[5] Erturk A, Vieira W G R, De Marqui C Jr and Inman D J 2010 On the energy harvesting potential of piezoaeroelastic systems *Appl. Phys. Lett.* **96** 184103

[6] Beeby S P, Tudor M J and White N M 2006 Energy harvesting vibration sources for microsystems applications *Meas. Sci. Technol.* **17** R175–95

[7] Roundy S and Wright P K 2004 A piezoelectric vibration based generator for wireless electronics *Smart Mater. Struct.* **13** 1131–44

[8] Glynne-Jones P, Tudor M J, Beeby S P and White N M 2004 An electromagnetic, vibration-powered generator for intelligent sensor systems *Sensors Actuators* A **110** 344–9

[9] Mitcheson P, Miao P, Start B, Yeatman E, Holmes A and Green T 2004 MEMS electrostatic micro-power generator for low frequency operation *Sensors Actuators* A **115** 523–9

[10] Wang L and Yuan F G 2008 Vibration energy harvesting by magnetostrictive material *Smart Mater. Struct.* **17** 045009
[11] Anton S R and Sodano H A 2007 A review of power harvesting using piezoelectric materials (2003–2006) *Smart Mater. Struct.* **16** R1–21
[12] Erturk A and Inman D J 2011 *Piezoelectric Energy Harvesting* (Chichester: Wiley)
[13] Christodoulou L and Venables J D 2003 Multifunctional material systems: the first generation *J. Miner. Met. Mater. Soc.* **55** 39–45
[14] Aglietti G S, Schwingshackl C W and Roberts S C 2007 Multifunctional structure technologies for satellite applications *Shock Vib. Dig.* **39** 381–91
[15] Thomas J P and Qidwai M A 2005 The design and application of multifunctional structure-battery materials systems *J. Miner. Met. Mater. Soc.* **57** 18–24
[16] Dong S, Zhai J, Li J F, Viehland D and Priya S 2008 Multimodal system for harvesting magnetic and mechanical energy *Appl. Phys. Lett.* **93** 103511
[17] Töreyin H, Topal E and Külah H 2010 A multi-source micro power generator employing thermal and vibration energy harvesting *Procedia Eng.* **5** 1176–9
[18] Anton S R, Erturk A and Inman D J 2010 Multifunctional self-charging structures using piezoceramics and thin-film batteries *Smart Mater. Struct.* **19** 115021
[19] Mayer P M and Ram R J 2006 Optimization of heat sink limited thermoelectric generators *Nanoscale Microscale Thermophys. Eng.* **10** 143–55
[20] Cobble M H 1995 Calculations of generator performance *CRC Handbook of Thermoelectrics* (New York: CRC Press) chapter 39
[21] Erturk A and Inman D J 2009 An experimentally validated bimorph cantilever model for piezoelectric energy harvesting from base excitations *Smart Mater. Struct.* **18** 025009
[22] Shu Y C and Lien I C 2006 Analysis of power outputs for piezoelectric energy harvesting systems *Smart Mater. Struct.* **15** 1499–502
[23] Stanton S C, Erturk A, Mann B P and Inman D J 2010 Nonlinear piezoelectricity in electroelastic energy harvesters: modeling and experimental identification *J. Appl. Phys.* **108** 074903
[24] Stanton S C, Erturk A, Mann B P and Inman D J 2010 Resonant manifestation of intrinsic nonlinearity within electroelastic micropower generators *Appl. Phys. Lett.* **97** 254101
[25] Kong N, Ha D S, Erturk A and Inman D J 2010 Resistive impedance matching circuit for piezoelectric energy harvesting *J. Intell. Mater. Syst. Struct.* **21** 1293–302
[26] Lallart M and Guyomar D 2008 An optimized self-powered switching circuit for non-linear energy harvesting with low voltage output *Smart Mater. Struct.* **17** 035030
[27] Thomas J P, Qidwai M A and Kellogg J C 2006 Energy scavenging for small-scale unmanned systems *J. Power Sources* **159** 1494–509